Validation Plots From a Simulation of the ANITA Experiment

Stephen Hoover, Amy Connolly, David Saltzberg
March 25, 2005

Abstract

We present a first pass at a set of plots made to test the inner workings of a Monte Carlo simulation of the ANITA experiment.

1 Introduction

A root script has been created to gather and display some of the intermediate data from a Monte Carlo simulation [1] of the ANITA and ANITA-Lite experiment. We assume that the reader is already familiar with the features of the Monte Carlo described in that note. The Monte Carlo has several components, among them simulations of the Antarctic continent, the Cherenkov radiation emitted from the neutrino shower, and the balloon payload itself. Creation of plots of these and other elements of the Monte Carlo help us understand that the implemented physics is essentially correct. The plots will also assist in the validation of new versions of the code.

Unless otherwise indicated, all plots display the sum of weights for passing events. The weighting takes into account neutrino attenuation through the Earth, biases due to selection of ν direction, and other such effects. Most 2-D histograms use totals of event weights for their temperature dimension (i.e. blue to red). Also unless otherwise indicated, plots are made with neutrinos of energy 10^{20} eV. (A higher energy allows for more events and greater electric fields, making features of the plots easier to observe. The root script allows for creation of plots at all energies.) Plots have been made with no noise in the antennas, no slopeyness on the surface of the firn, and no rays reflecting from the bottom of the ice. The Monte Carlo is run by default with these options enabled, but turning them off for this study allows better observation of the other contributing effects. Monte Carlo code version 1.20 with minor modifications was used to produce the data examined in this note.

2 Plots of Locations of the Neutrino Interactions

2.1 Position of Interaction

Figure 1 is an overhead view of the Antarctic continent. Note that this is not a scatter plot, but rather a finely binned histogram. The color of the bins represents the sum of weighted numbers of interactions from that location. The black line is the path of the balloon used inside the program, in this case, GPS data taken from the ANITA-Lite flight.

For lower energies (see fig. 2), we can see the detected events clustering around the balloon path, showing the characteristic distance at which neutrinos can be detected. The blockiness that becomes apparent at higher neutrino densities (due solely to larger numbers of neutrinos detected) results from the paramatrization of the physical Antarctica that was used - data on ice thickness, etc., is in bins of 2° latitude by 2° longitude. Areas from which no neutrinos are detected, in the upper left and lower portions of the plot, correspond to regions of the continent in which ice is thin or nonexistent. We are working to verify that no significant amount of ice has been omitted from the simulation. The hard cutoff which becomes clearly apparent on the right at energies of 10^{20} eV and above is the edge of the continent. Past this circle, there is no ice in which to detect neutrinos.

2.2 Depth of Interaction

Figure 3 shows the depth at which each neutrino interacts. The greatest number of events are detected from shallow depths, with numbers decreasing as one looks deeper. This is due to RF attenuation within the ice. Neutrinos of greater energy produce larger electric fields, and so can be detected deeper, as seen in figure 4.

2.3 Surface Distance of Interaction from Balloon

Figure 5 shows how far along the surface of the continent each neutrino that was detected was from the balloon. This plot is the product of two effects. First, the RF has a $1/r$ dependence. This reduces the number of events detected far from the balloon, and increases the number of events seen close to the balloon, where the signal will be stronger. Second, the plot displays phase space effects. There is more volume in which interactions can occur further from the balloon, which results in fewer detections close to the balloon, and more detections further away. In Figure 6, the square of the surface distance is plotted to remove phase space effects. Here the primary remaining effect is the $1/r$ dependence of the RF. Even with phase space removed, however, the number of events at the very closest distances cuts off. This is because the balloon's antennas are pointed at the horizon, and therefore recieve less signal from events directly below them, and also because the upcoming neutrinos which would direct RF upwards toward the balloon are shielded by the Earth. The latter effect dominates.

2.4 Surface Distance of Interaction from Balloon versus Depth

Figure 7 is a combination of figures 4 and 5. Figure 8 is the same plot with phase space effects removed. The difficulty of detecting neutrinos directly below the balloon can be seen, as well as the effects of RF attenuation in the ice.

2.5 Angle of Incoming Neutrino

Figure 9 displays the angle between the momentum of the incoming neutrino and the plane of the surface above the point of interaction. Two effects restrict the possible angles. First, the direction of the incoming neutrino determines the direction of the Cherenkov cone emitted from the resulting shower. If the neutrino is angled too sharply down, emitted RF will strike the firn-air interface at too steep of an angle and undergo total internal reflection. This causes the sharp cutoff observed on the downgoing neutrinos.

The second contributing effect is attenuation of the neutrinos inside the Earth. This produces the trail of upgoing neutrinos on the left side of the graph. The more steeply upgoing the neutrino, the more of the Earth it must pass through, and therefore the higher its chances of being absorbed on the way. Lower energy neutrinos have less chance of being absorbed, and so more of them are detected coming up, as seen in figure 10. The glitches around -12° and the 0° cutoff at low energy are not yet understood.

3 Plots Relating to RF in Ice and in Air

Some plots in this section reference the "ice-firn pseudo-interface". There is no abrupt transition between the ice and the firn, but the gradual transition over a region can be modeled by a single interface. References to the ice-firn pseudo-interface, then, represent the changes in the RF between its point of origin and the top of the firn.

3.1 Fresnel Coefficient at Firn-Air Interface

Figure 11 displays the Fresnel coefficent (accounting for polarization) applied to the RF as it leaves the ice, relative to the angle with respect to the surface normal. (Local down refers to be a vector from the point of interaction to the center of the Earth. As the plot was made with no surface slopeyness, the angle is here identical to the angle at which the RF strikes the surface of the ice.) As expected, the coefficient is large for the few rays that leave nearly straight up, and goes to zero as the incident angle approaches the critical angle. (The critical angle at this transition is 50°.) Figure 12 is the projection onto the y-axis.

3.2 Refraction at Boundaries

Figure 13 displays the incident angle of the RF on the firn-air interface versus the refracted angle of the RF in air. This is just Snell's law. Figure 14 is a similar plot for the ice-firn pseudo-interface. In each case, the critical angle can be seen. (Approximately 50° at both the firn-air interface and at the ice-firn pseudo-interface.) Note that most rays approach the firn-air boundary at nearly the critical angle, and so are bent almost parallel to the ground. Note also that at the ice-firn pseudo-interface, no rays are seen to refract more than 50° from the normal. This is because those rays that do bend further undergo total internal reflection at the next boundary, and so are never observed at the balloon.

3.3 RF Direction in Air

Figure 15 is a plot of the three-dimensional angle between the direction of RF propagation in air and the momentum of the neutrino. Figure 16 includes the relative azimuthal angle of the RF as well, with $\phi = 0^\circ$ being the direction away from the ground. All detected RF is going up from the neutrino momentum - RF going down goes further into the ice and is lost.

4 Plots Relating to Antennas

4.1 Antenna Detecting Maximum Signal

Figure 17 shows which antenna on the balloon detected the maximum signal in each event. The antenna with the maximum signal is taken for each of the balloon's three layers of antennas, so each event generates three entries on the plot. The top layer consists of antennas 0-7, the middle layer antennas 8-15, and the bottom layer antennas 16-31. Since the bottom layer contains twice as many antennas as the top two, each antenna in the bottom layer is half as likely to be the antenna that reads the maximum signal.

4.2 Triggers per Antenna

Figure 18 looks at the total number of lowest level triggers (channels more than 2.3 times expected noise, see ref. [1]) counted on each antenna over the entire program run. Note that a single event can trigger up to 8 channels on an antenna, and several antennas will be hit for each event. As on the previous plot, differences decrease with more events.

4.3 Triggers for Two Random Events

Figures 19 and 20 display the number of channels passing the lowest level trigger on each antenna for a randomly chosen event. Each antenna has 8 channels (4 frequency bands, 2 polarizations per band). We can see the antennas pointing toward the event on each of the three layers recieving more signal.

4.4 Angle of RF with Antenna

Figure 21 shows the three dimensional angle between the RF and the normal to the antenna that saw the largest signal on the first layer. Most signals are detected within about 25° of the antenna normal, since signals at a larger angle than that will cause the maximum signal to be on a different antenna. (There are 8 antennas on layer 1, so signals with a horizontal angle over 22.5° should be detected on the next antenna. Some signals do come from slightly further - this is not yet understood. Perhaps due to polarization effects.) The antennas are at a cant angle of 10°, and the horizon is at a cant of 7°. Events come in with an angle of 0° if they are directly ahead of the antenna, which is only true for a single distance. (Here approximately 220 km, or 50,000 km^2, and blurred slightly due to altitude fluctuations over the flight of the balloon.) Events directly below the balloon will have a large three-dimensional angle with the antenna detecting the maximum signal. The same plot for layer 2 looks identical, save for noise. The plot for layer 3, figure 22, is half as thick because there are twice as many antennas.

In figure 23, the incoming RF direction is shown in terms of the angle to the E-plane and the angle to the H-plane on the antenna seeing the maximum signal (layer 1). The angle with respect to the H-plane is an "up and down" angle, an angle of rotation about the horizontal axis of the antenna. The angle with respect to the E-plane is the "side to side" angle, an angle of rotation about the antenna's vertical axis. This plot is shaped by the same factors that shaped the previous plot. The side-to-side spread is limited by how far one can go before another antenna is closer. (The waist at 0° is not yet understood, however.) Most events come from a small vertical angle because most area is far from the antenna. Only a few events come from large angles. Again, the plot for layer 3, figure 24, is half as thick because layer 3 has twice as many antennas.

Figures 25 and 26 have the same information as the previous two plots presented in different coordinates. Theta is the three dimensional angle of the incoming RF with respect to the beam of the antenna with the maximum signal. Phi is an azimuthal angle. $\phi = 0$ is upward, $\phi = \pm 90$ is to the side, and $\phi = \pm 180$ is downward. These plots are difficult to understand upon first viewing; comparisons with figures 23 and 24 are helpful here.

5 Miscellaneous Plots

5.1 Neutrino Flavors

Figure 27 shows the distribution of neutrino flavors producing the events detected at the balloon. Figure 28 is a similar plot for neutrino energies of $10^{18.5}$ eV.

5.2 Banana Plot

Figure 29 is the "banana" plot, named for the shape seen in the plot. It is an image of the RF signal emitted by the shower. The plot shows the result of a muon neutrino neutral current event at 2×10^{19} eV, upcoming at 0.413° from the horizontal and interacting at a depth of 400 meters. The event elasticity was 0.2, and it was observed from a distance of 600 km.

The RF is emitted in a Cherenkov cone, producing the arc visible in the plot. Rays bent closer to the ground lose more power to fresnel and magnification factors, accounting for the arc's tapering off before it reaches the ground. The notch on the right side of the plot is not yet understood.

6 Conclusion and Future Plans

Creation of the validation plots has been valuable. They have allowed several improvements to be made in the code, and given confidence in the effective volume $\times$ steradians output of the Monte Carlo. Some minor features in the plots are not yet understood, and investigation continues into the origin of these features.

Future plans include the creation of plots for a larger variety of input parameters, as well as the expansion of the root script to include more validation plots. Some planned additional plots are studies of the magnification factor at the firn-air interface and ice-firn pseudo-interface, as well as an examination of the RF polarization vectors relative to detecting antennas.

References

[1] A. Connolly, Anita Note ♯17, "Summary of a Simulation of the ANITA Detector"

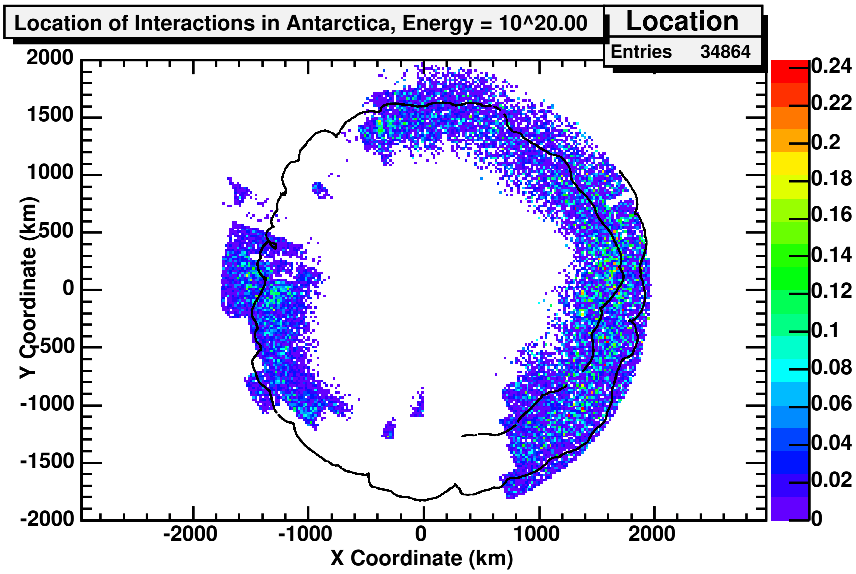

Figure 1: Location of detected neutrino interactions on Antarctica. (Neutrino energy 10^{20} eV.) The balloon path is superimposed.

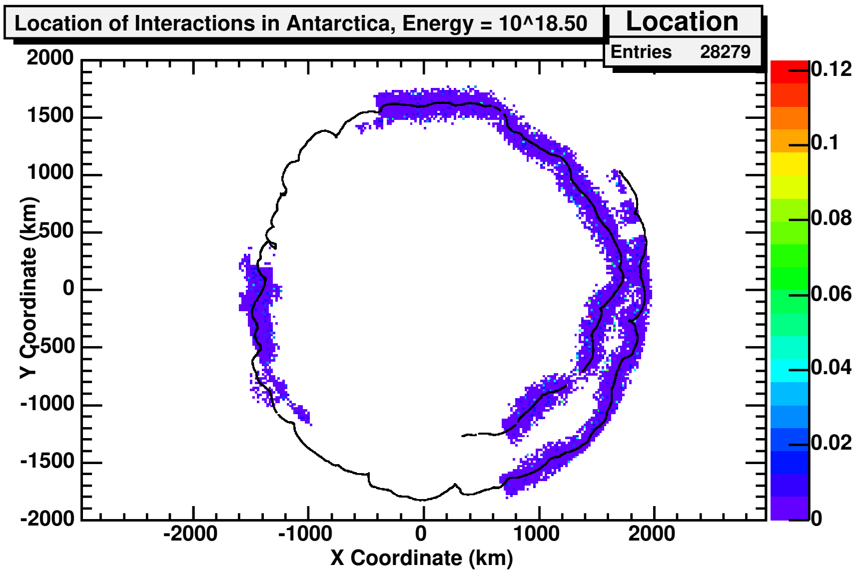

Figure 2: Location of detected neutrino interactions on Antarctica. (Neutrino energy $10^{18.5}$ eV.) The balloon path is superimposed.

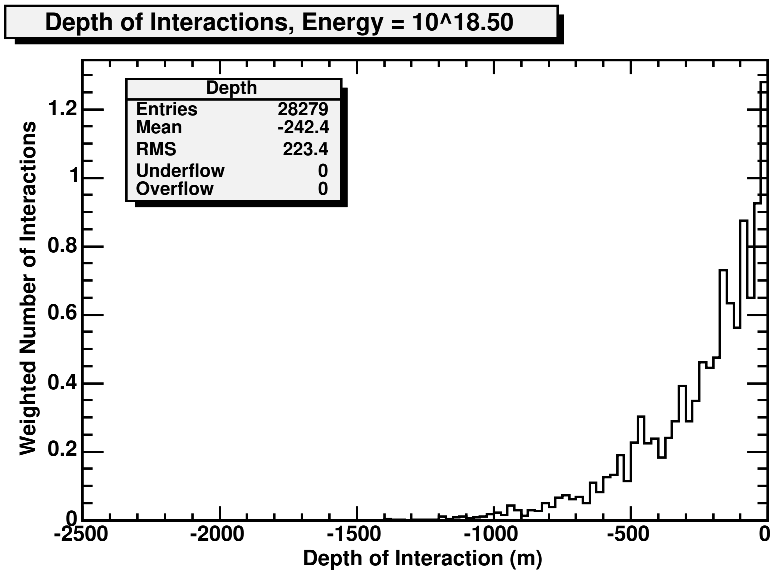

Figure 3: Depth under ice of interactions that were detected at the balloon. (Neutrino energy $10^{18.5}$ eV.)

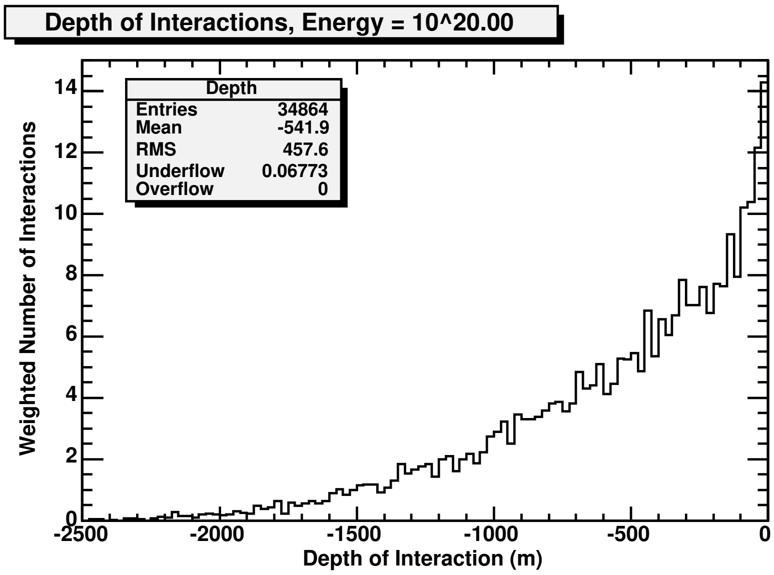

Figure 4: Depth under ice of interactions that were detected at the balloon. (Neutrino energy 10^{20} eV.)

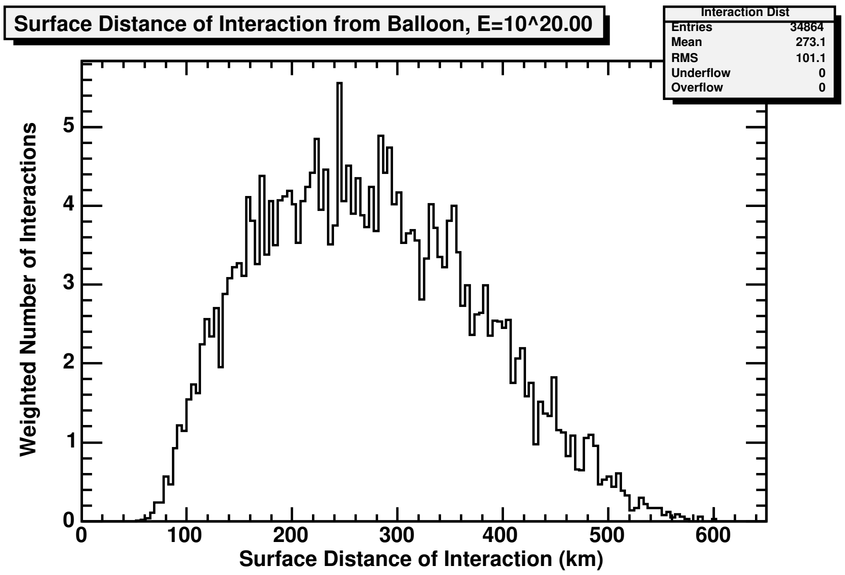

Figure 5: Surface distance from balloon of interactions that were detected.

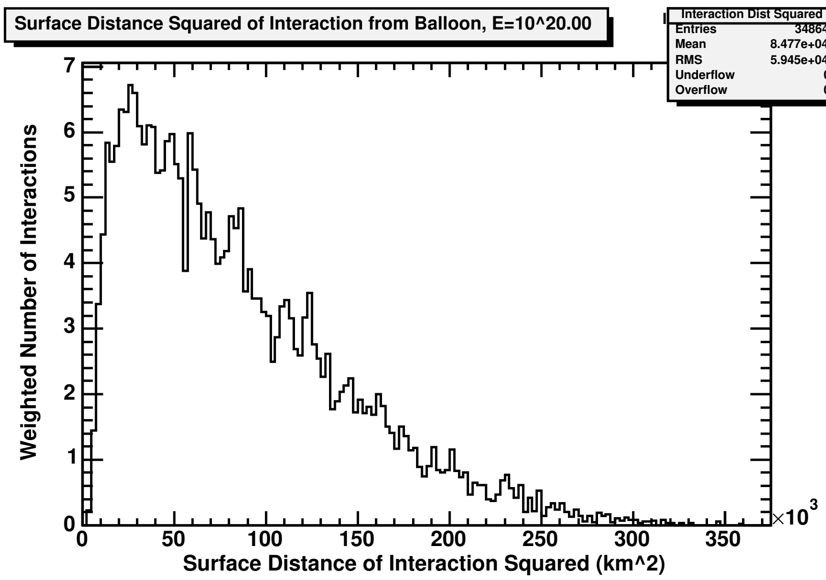

Figure 6: Surface distance squared from balloon of interactions that were detected.

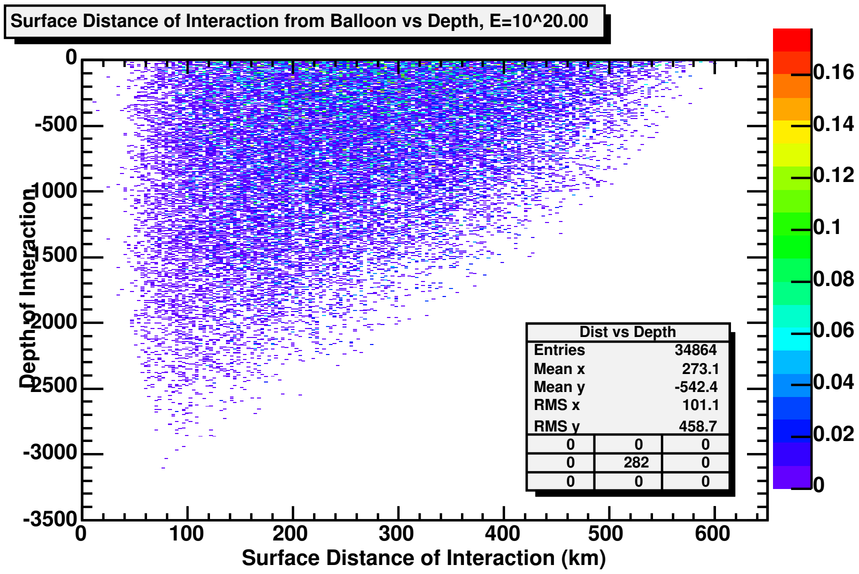

Figure 7: Surface distance from balloon of interactions that were detected versus depth of interaction.

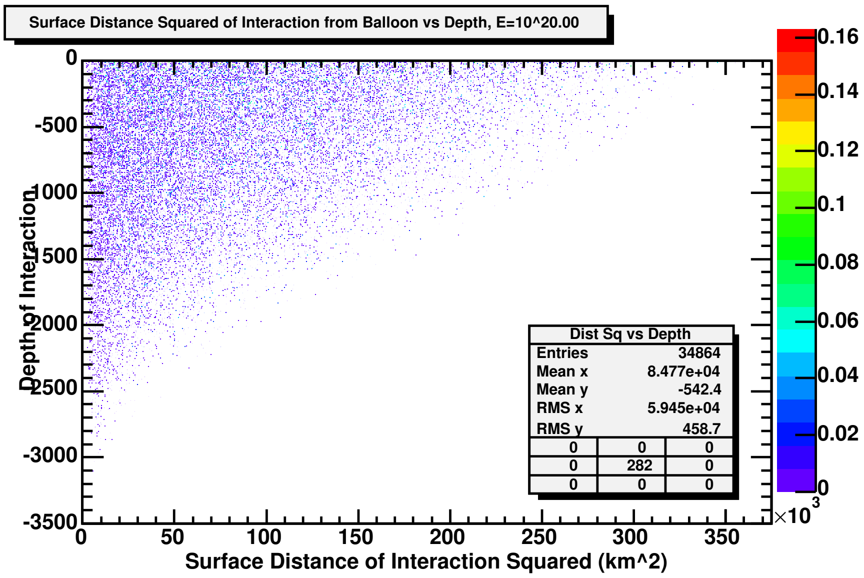

Figure 8: Surface distance squared from balloon of interactions that were detected versus depth of interaction.

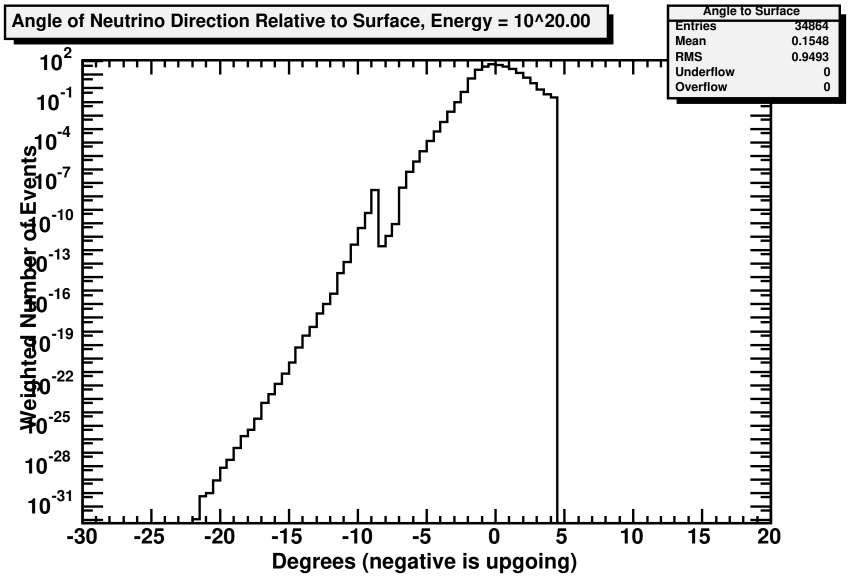

Figure 9: Angle of incoming neutrino momentum with plane of surface, neutrino energy 10^{20} eV. Negative angles are upcoming neutrinos, positive angles are downgoing.

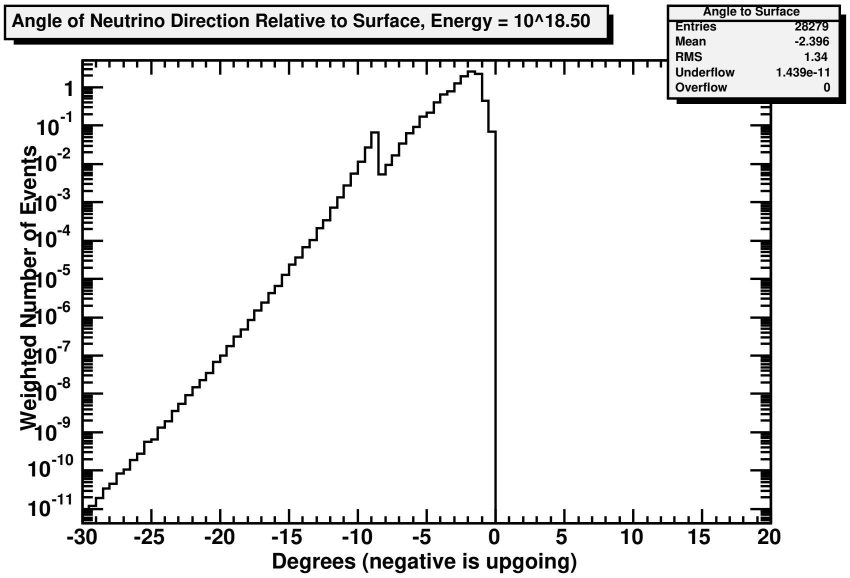

Figure 10: Angle of incoming neutrino momentum with plane of surface, neutrino energy $10^{18.5}$ eV. Negative angles are upcoming neutrinos, positive angles are downgoing.

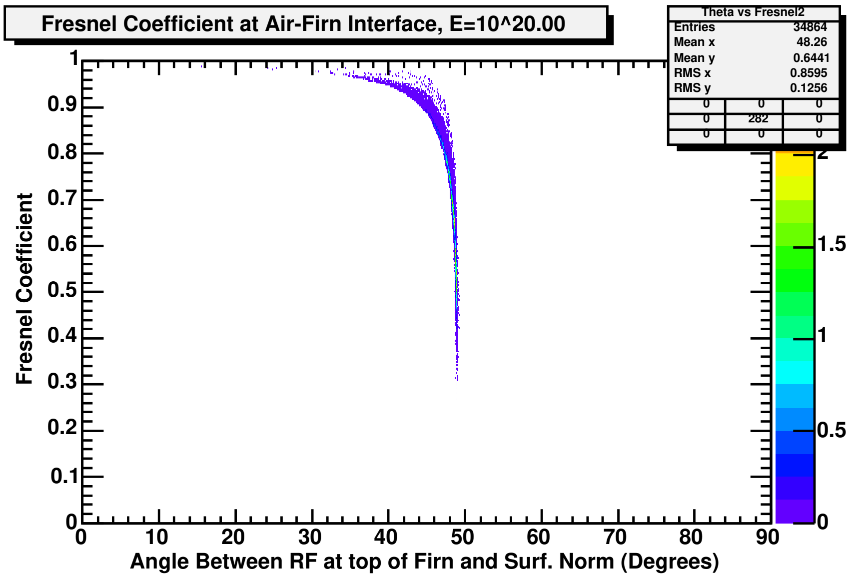

Figure 11: Angle of RF with normal of firn-air interface versus frenel coefficient applied.

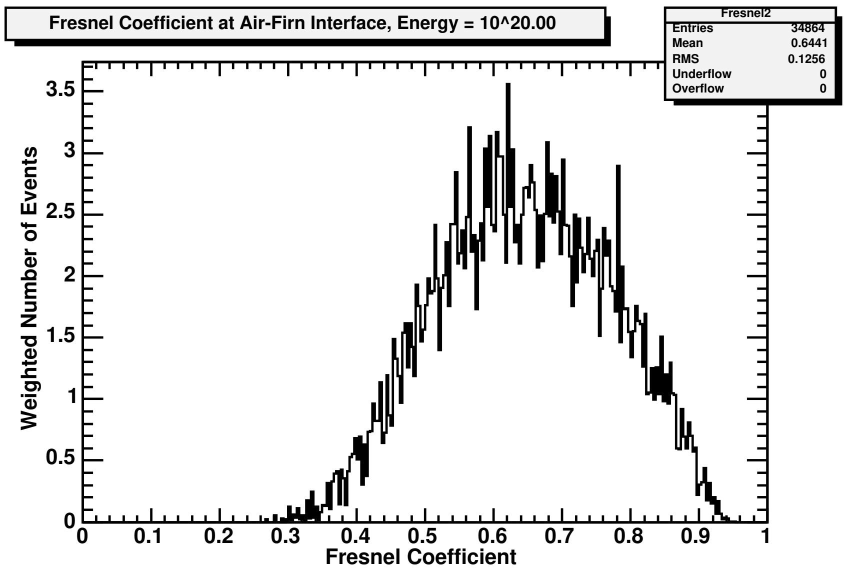

Figure 12: Fresnel coefficient applied to RF as it passes through firn-air interface.

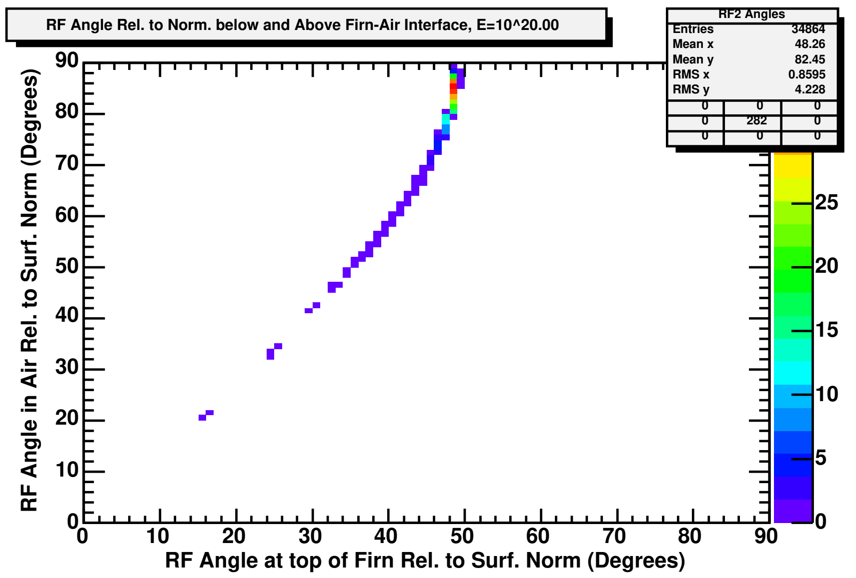

Figure 13: Angle of RF with surface normal before and after refracting through firn-air interface.

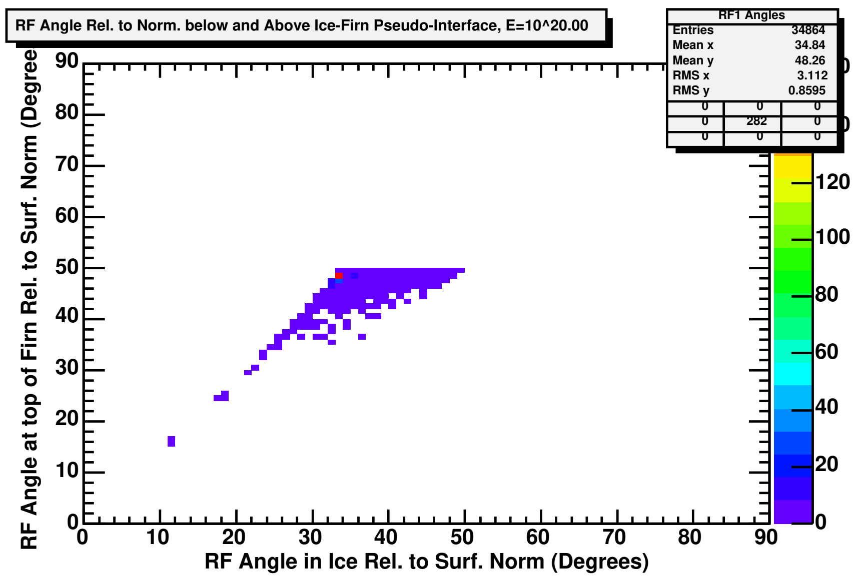

Figure 14: Angle of RF with surface normal before and after refracting through ice-firn pseudo-interface.

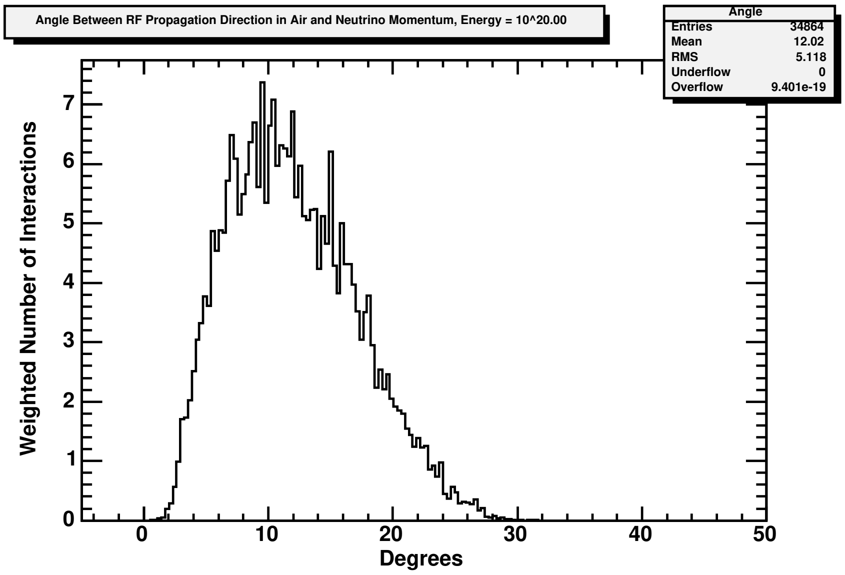

Figure 15: Three dimensional angle between detected RF and momentum of originating neutrino.

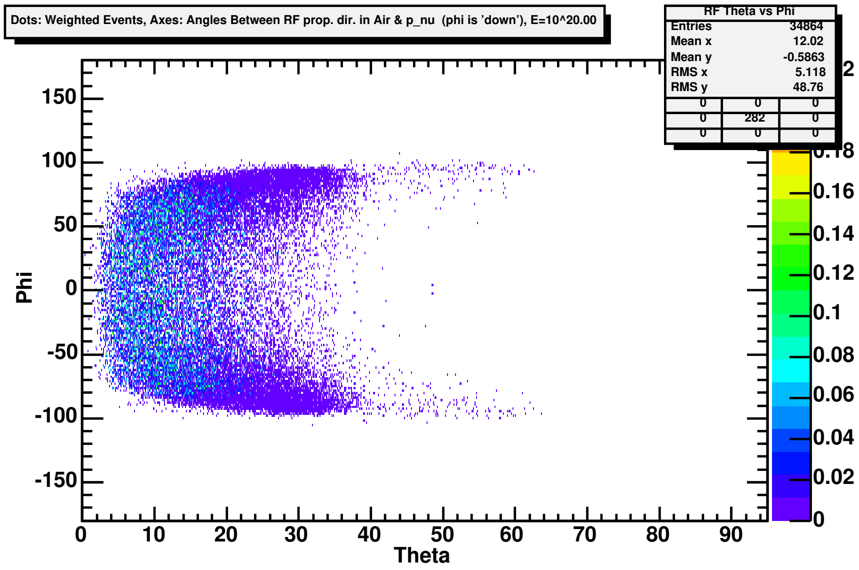

Figure 16: Direction of detected RF with respect to momentum of originating neutrino. Theta is the three dimensional angle between the two vectors, and phi is an azimuthal angle. $\phi = 0$ is up.

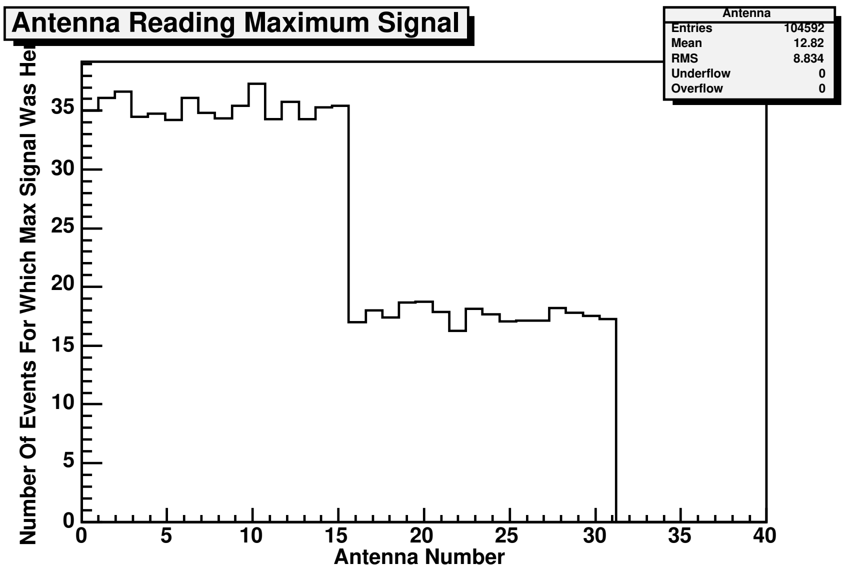

Figure 17: How many (weighted) times each antenna was the one to detect the maximum signal. Antennas 0-7 are the top layer, 8-15 are on the middle layer, and 16-31 are on the lowest layer of the balloon.

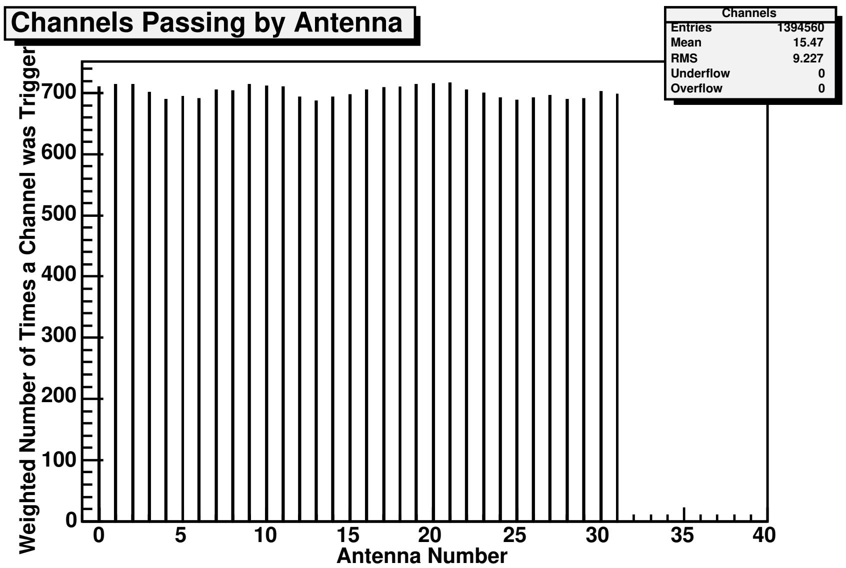

Figure 18: How many (weighted) times each antenna had a channel pass the lowest level trigger.

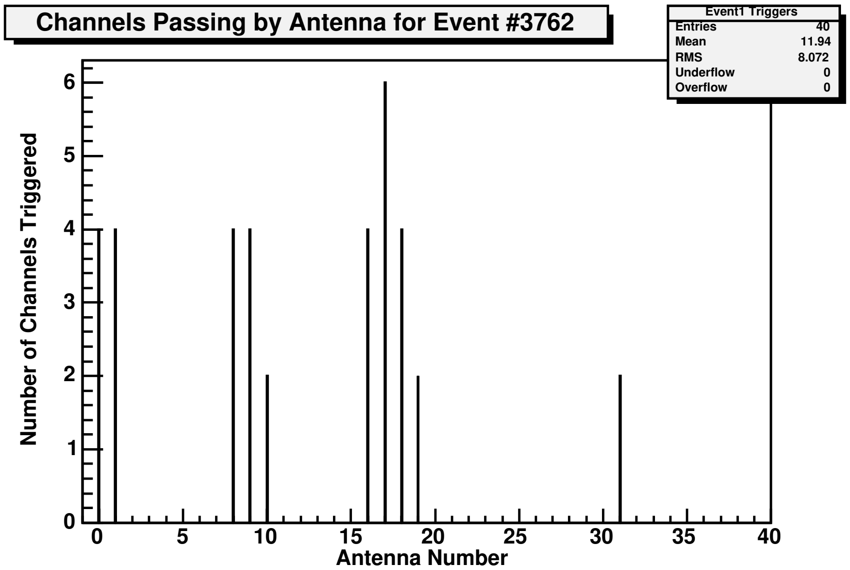

Figure 19: How many triggers each antenna recieved for a randomly chosen event.

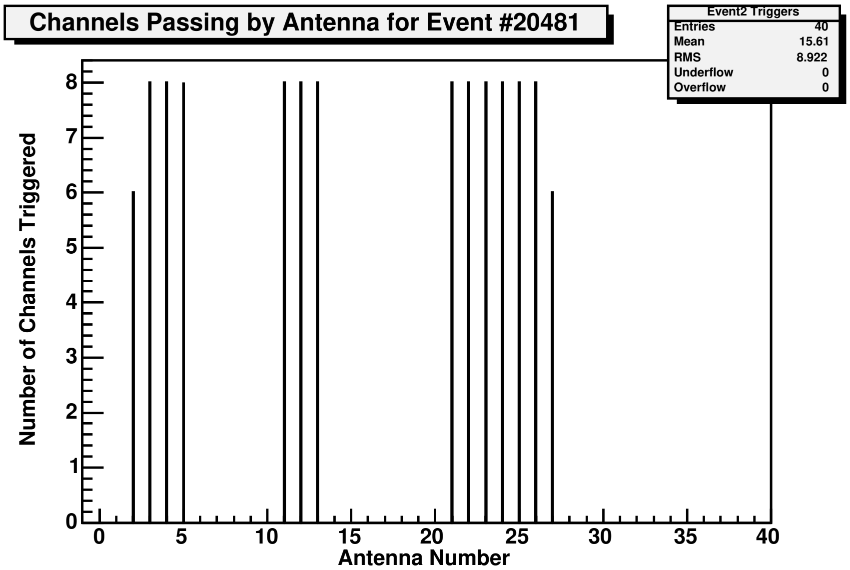

Figure 20: How many triggers each antenna recieved for a randomly chosen event.

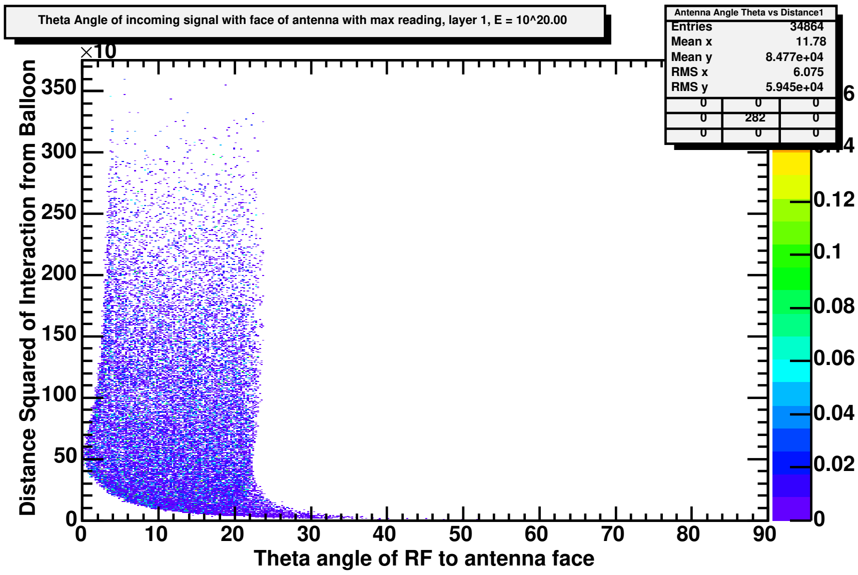

Figure 21: Three dimensional angle of RF with beam of antenna seeing maximum signal in the first layer versus surface distance squared of interaction from the balloon. Y-axis is given in units of $km^2 \times 10^3$.

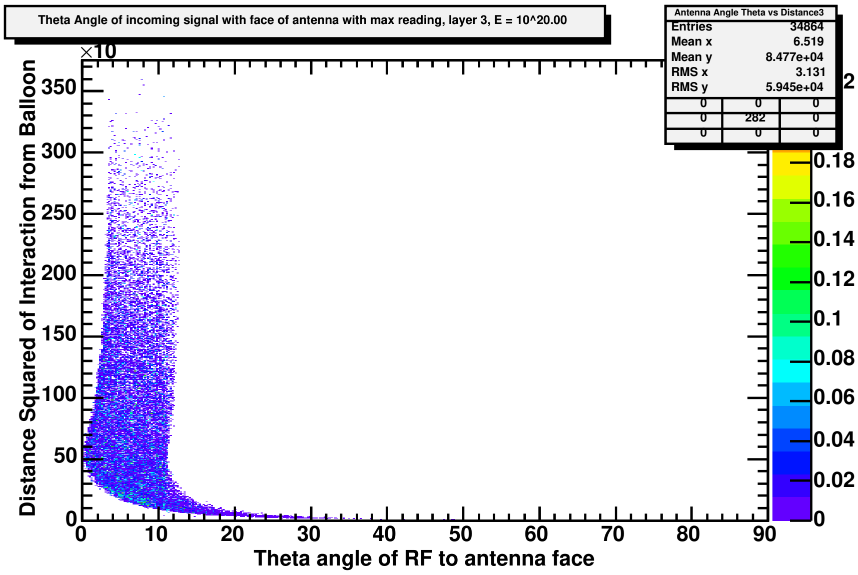

Figure 22: Three dimensional angle of RF with beam of antenna seeing maximum signal in the third layer versus surface distance squared of interaction from the balloon. Y-axis is given in units of $km^2 \times 10^3$.

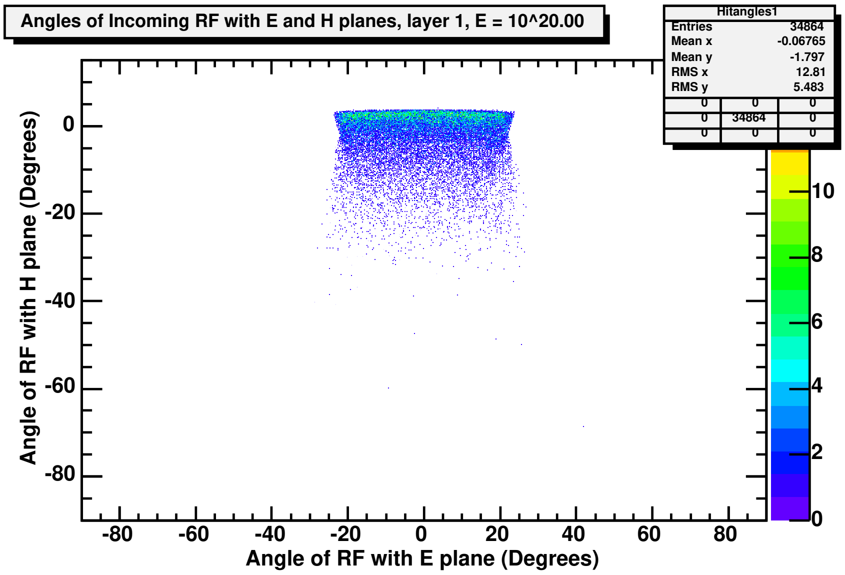

Figure 23: RF angles on antenna seeing maximum signal, layer 1: angle of rotation about antenna vertical axis (E-plane) versus angle of rotation about antenna horizontal axis (H-plane).

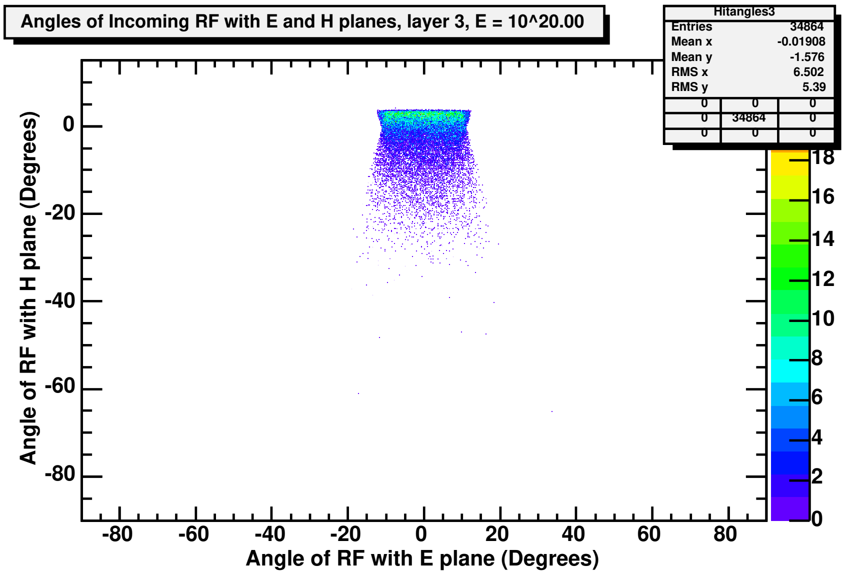

Figure 24: RF angles on antenna seeing maximum signal, layer 3: angle of rotation about antenna vertical axis (E-plane) versus angle of rotation about antenna horizontal axis (H-plane).

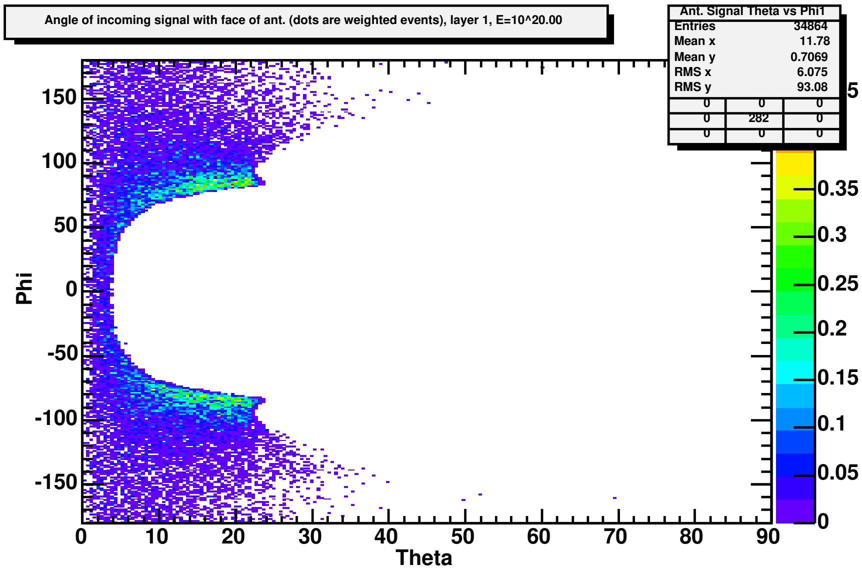

Figure 25: RF angles on antenna seeing maximum signal, layer 1: 3-D angle versus azimuthal angle, $\phi = 0$ upward.

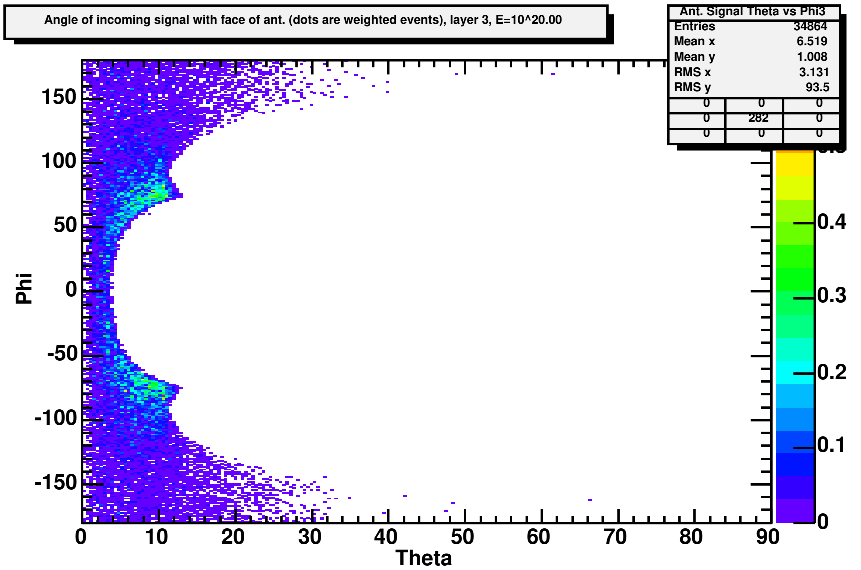

Figure 26: RF angles on antenna seeing maximum signal, layer 3: 3-D angle versus azimuthal angle, $\phi = 0$ upward.

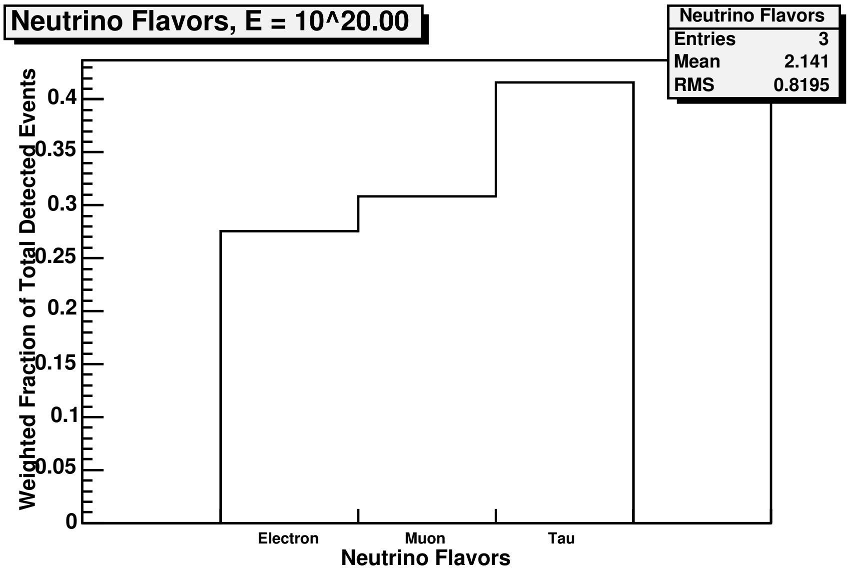

Figure 27: Fraction of detected events originating from each flavor of neutrino. Neutrino energy 10^{20} eV.

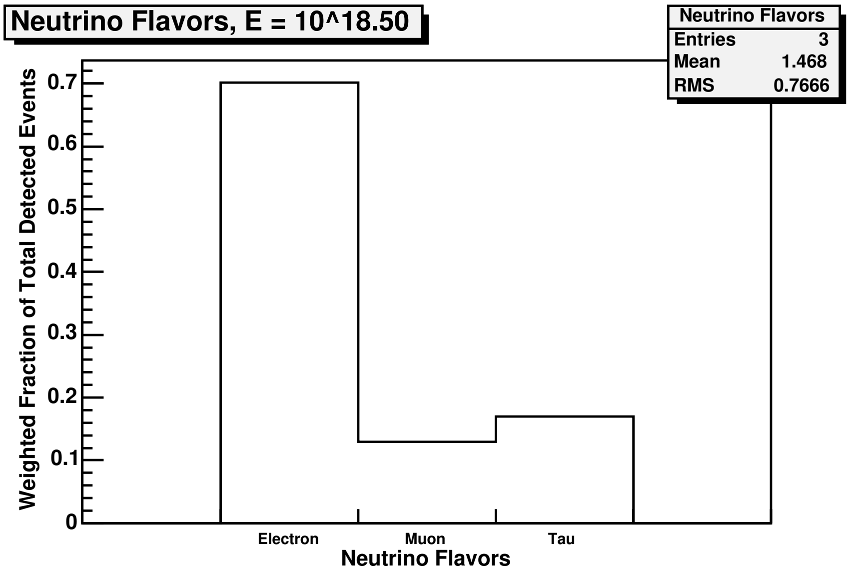

Figure 28: Fraction of detected events originating from each flavor of neutrino. Neutrino energy $10^{18.5}$ eV.

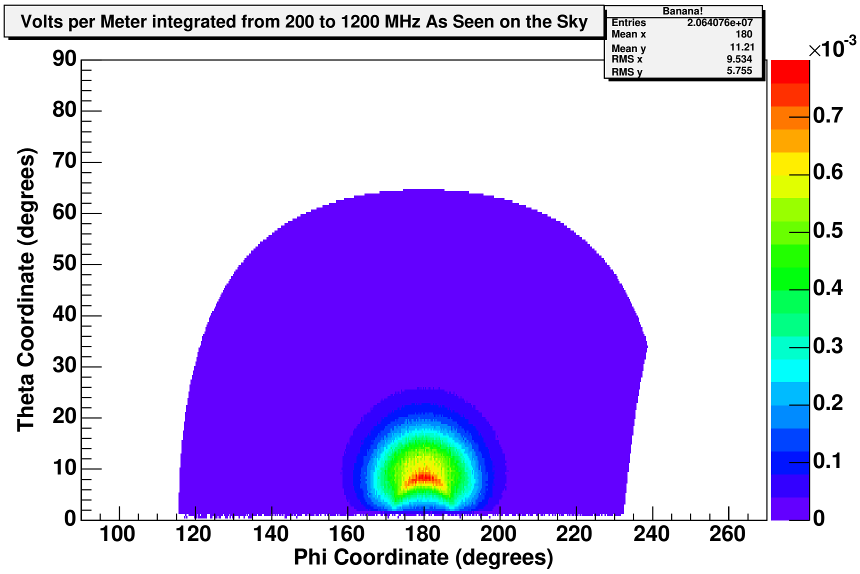

Figure 29: Volts per meter, integrated from 200 to 1200 MHz, as seen 600 km away from the interaction point. θ is the polar angle, measured from the ground. ϕ is the azimuthal angle, with $\phi = 180$ being straight ahead of the neutrino.